Detailed Modeling of Pneumatic Braking in Long Combination Vehicles

Zichen Zhang - *Virginia Tech, USA* ,
Nan Sun - *Virginia Tech, USA* ,
Yang Chen - *Virginia Tech, USA* ,
Mehdi Ahmadian - *Virginia Tech, USA*

Abstract

A detailed model for pneumatic S-cam drum brake systems is developed and integrated into a multibody dynamic model for a 33-ft A-double long combination vehicle (LCV). The model, developed in TruckSim®, is used to study the dynamics of LCVs during straight-line braking at various speeds. It includes the response delay in braking that occurs from the time of application to when the brakes are applied at the drum for all axles. Additionally, the model incorporates an accurate characterization of brake torque versus chamber pressure at different speeds, along with the anti-lock brake system (ABS) dynamics, to yield an accurate prediction of the vehicle's deceleration during braking. The modeling results are compared with test results at speeds ranging from 20 to 65 mph on dry pavement. A close match between the model's prediction and test results is observed. The model is then used to perform a parametric study that evaluates braking distance and time for different pavement coefficients of friction (μ_p) at various speeds. The results indicate a distinct nonlinear relationship between μ_p and braking dynamics. At various μ_p, stopping time increases linearly with speed, as perhaps expected. Stopping distance, however, increases nonlinearly for larger μ_p and linearly for smaller μ_p versus speed. At a given speed, stopping time increases nonlinearly with reduced μ_p, whereas stopping distance increases relatively linearly with reduced μ_p.

Keywords: long combination vehicle; pneumatic brake; brake model; brake delay; brake torque; straight-line; braking distance; braking time; longitudinal dynamics; drum brake

1. Introduction

Long combination vehicles (LCV) consist of a tractor and two or more trailers that are connected through a fifth wheel and or pintle hook. LCVs are commonly used for short- to medium-haul transport of goods to and from a loading station to a central hub. Their modular flexibility often provides operational efficiencies relative to tractor-semitrailers with a single, longer trailer [1,2]. LCVs are equipped with pneumatically actuated brakes, as opposed to hydraulic brakes that are common on automobiles and light trucks [3, 4]. Pneumatic brakes use air as the working fluid to actuate the brakes on each axle. Due to the air's transport delay, there is a short but measurable delay between the braking application at the pedal and when the brake shoes engage with the drum. This delay is directly proportional to the axle distance from the brake reservoirs and is greatly influenced by the pressure drops at various valves and regulators that are part of a pneumatic system. More than 85% of commercial trucks in the U.S. use the S-cam drum brake [3], which is also the focus of this study. As compared to the disc brakes, drum brakes have lower costs but are more prone to brake fading that could occur with repeated brake application, particularly at higher speeds [5].

Accurate modeling of braking in LCVs requires a precise and detailed model of the pneumatic brakes for all vehicle units. The LCV brake system typically includes a set of pneumatic components, such as air tanks, a treadle valve, relay valves, and brake chambers. Collectively, these components and the air pipes and fittings that connect them form the pneumatic brake system. The trailers are pneumatically connected to the tractor through gladhands that transfer air from the tractor to other units in the rear. Upon braking at the pedal by the driver, air travels through the brake system to increase the brake chamber pressure and press the brake shoes against the rotating drum with a force that is proportional to the chamber pressure and brake shoe travel. The time between the brake application at the pedal and full braking at the drum is referred to as brake delay [6-8]. LCVs have different units and for each, the brakes are engaged sequentially with time delays. The time delay for the rear units increases with increasing length and number of units. With increasing chamber pressure, the brake shoe travels farther and presses the shoes against the drum with increasing force, hence generating larger brake torque and higher deceleration. As stated earlier, the accuracy of braking torque vs. application pressure and delays are most critical to accurate modeling of braking dynamics. In this study, special care has been taken to include an accurate account of both the brake delay and torque in a detailed model that is developed and integrated into TruckSim®.

Braking at higher speeds would result in increased temperature at the brake shoes and drum that could affect the braking performance, particularly at higher temperatures that would reduce the brake shoe coefficient of friction and increase the diameter of the drum [9 – 11]. The resulting loss of braking effort due to heat buildup at the brakes is commonly referred to as brake fading. Brake fading occurs more substantially with repeated braking at higher speeds for which the larger kinetic energy results in larger thermal energy. This happens both in between brake cycles and during each cycle. Hence, the reduction in braking torque (force) that occurs due to temperature build-up at the shoe and drum must also be considered in the model, as is done in this study.

The majority of the past braking studies for commercial vehicles have focused on semitrucks with a single trailer [3, 10, 12 – 19]. Some have not included the brake delay that occurs in such vehicles, and even more prominently in LCVs that are considered here. Without including the detailed effect of the delays and brake torque reduction at higher initial speeds due to temperature build-up, a model would not yield sufficiently accurate results.

This paper develops a detailed dynamic model of the pneumatic brake system for LCVs, namely, a tractor and two 33-ft trailers that are connected with an "A" convertor-dolly. As shown in Figure 1, this combination is commonly known as "33-ft A-double," [20 - 22]. To determine the integration of the pneumatic brake model into a general-purpose multi-body dynamic code, TruckSim® is coupled with the pneumatic brake model through a co-simulation technique. The coupled pneumatic-brake vehicle-dynamics model is validated by comparing the simulation results with test data on a vehicle with the same configuration. Using the validated model, a parametric study is performed to determine the effect of road conditions on braking distance and time at different speeds.

It is important to note that the study does not include the effect of aerodynamics drag on braking distance and time, which is expected to decrease both. It is our best estimate that including aerodynamics drag would decrease the stopping distance and time by one percent or less.

As stated earlier, the primary focus of the study will remain on developing accurate brake models that include the effect of pneumatic delays and ABS, for predicting braking time and distance during emergency or accident avoidance braking with reasonable accuracy.

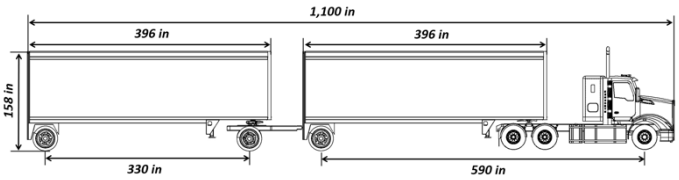

Figure 1. Tractor, two 33-ft trailers, and an "A" converter dolly, commonly referred to as "33-ft A-double"

2. Brake System Model Development

2.1 Pneumatic Components in the Brake System

The modeling of pneumatic brake systems requires some knowledge of their pneumatic components and working principle. Figure 2 schematically shows the plumbing configuration of the pneumatic brake system in the 33-ft A-double. The main components included in the brake system are:

a) Air tanks
b) Treadle valve
c) Relay valves
d) Brake chambers
e) Brake shoes and drum

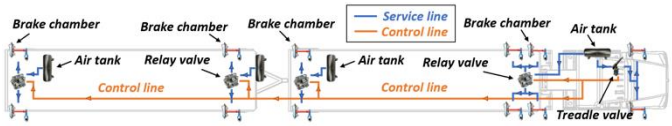

Figure 2. Top view of the brake system plumbing in a 33-ft A-double

(a) Air Tank

The air tank receives and stores air from a compressor, and the air is used to charge the brake chamber and/or activate a relay valve. The pressure in the tank is maintained at a certain range specified by the compressor.

(b) Treadle Valve

The treadle valve is controlled by the brake pedal and acts as the brain of the system to control the air pressure provided to the brake chamber of the steering axle, and the relay valves of the other axles of the LCV. The treadle valve has primary and secondary service circuits. The primary circuit is actuated via pedal force to provide pressurized air to the relay valves of the tractor drive axle(s), the dolly, and the trailers' axles. The secondary circuit is actuated by the air delivered from the primary circuit to supply air to the steering axle brakes. If the primary circuit fails, the second circuit can be actuated directly by pedal force, such that the treadle valve can still work properly in case of such a failure. Federal regulations have required the use of dual-circuit treadle valves for heavy commercial vehicles since about 1975 [23].

(c) Relay Valve

The relay valve is used to speed up the brake application and brake release on the tractor, dolly, and trailers. It is typically installed, along with its own air tank, near the brake chamber, and a large diameter pipe is used between the service tank and the relay valve to minimize the resistance for the airflow into the brake chamber. The airline from the relay valve to the treadle valve is the control line that signals the relay valve to supply the necessary air pressure to the chamber. The relay valve also allows for a quick exhaust of air for the fast release of the brake [24].

(d) Brake Chamber

The brake chamber is the device capable of transferring the force of pressurized air to the mechanical linkage, as shown in Figure 3. When the compressed air flows into the brake chamber through the inlet port, it forces the diaphragm against the return spring and moves the push rod forward. If the air in the brake chamber is released, the return spring pushes the diaphragm and pushrod back to their initial position.

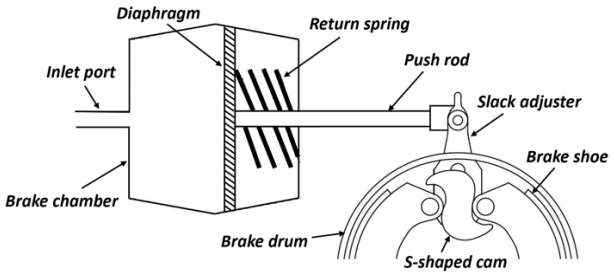

Figure 3. S-cam brake chamber and drum assembly

(e) Brake Shoes and Drum

During the brake application, the forward movement of the push rod is translated into the rotation of an S-shaped cam through a slack adjuster, as shown in Figure 3. Consequently, the high point acts against the cam roller, pushing the brake shoe out against the drum, generating brake torque to resist the rotation of the brake drum and wheel.

2.2 Working Principle of the Brake System

For the pneumatic brake system shown in Figure 2, upon the brake application at the pedal, the treadle valve opens to supply high-pressure air to the control line (marked in orange), while supplying air to the brake chambers on the steering axle. The pressure signal is then sent through the control line to the relay valves at the tractor drive axle(s), front trailer, dolly, and rear trailer sequentially. The relay valve in turn uses the compressed air in its dedicated air reservoir to charge brake chambers via the service line (marked in blue). The accumulated pressure in the brake chamber provides a mechanical force that pushes the brake shoes against the drum, generating brake torques on the wheel, as shown in Figure 3. Upon releasing the brake pedal, the air is vented out of the brake chamber and the pushrod retracts to release the brake shoes from contacting the drum.

To model brake application and release process, it can be broadly divided into three parts:

- Pneumatic subsystem modeling
- Brake torque modeling
- Anti-lock brake system (ABS) modeling

2.3 Pneumatic Subsystem Modeling

The response delay of the relay valve relative to the brake-valve activation can be represented by the following time-delay model [8]:

$$p_{c\_tractor}(t) = p_{brake}(t - \tau_1) \quad (1)$$

$$p_{c\_trailerA}(t) = p_{brake}(t - \tau_2) \quad (2)$$

$$p_{c\_dolly}(t) = p_{brake}(t - \tau_3) \quad (3)$$

$$p_{c\_trailerB}(t) = p_{brake}(t - \tau_4) \quad (4)$$

where $p_{c_{tractor}}$, $p_{c_{trailerA}}$, $p_{c_{dolly}}$, and $p_{c_{trailerB}}$ are the control pressure of the relay valve on the tractor, front trailer, dolly, and rear trailer,

respectively. p_{brake} is the pressure input of the system controlled by the brake valve, and τ_1, τ_2, τ_3, and τ_4 are the time delay of the control line for the tractor, front trailer, dolly, and rear trailer, respectively. The pressure loss and air transport delay in the air hoses are important causes of the control line delay [25]. In this study, the delay of the control line is determined through straight-line braking tests at various speeds for an identical 33-ft A-double. The test results of the brake pressure of the tractor and trailers for the test at 20 mph are shown in Figure 4, indicating the time delay between the rear trailer, front trailer, and tractor. The longer delay at the rear trailer is caused by the increased resistance due to longer air hoses (control lines) and additional valves in the path of the airflow [26]. A summary of time delays of all vehicle units (i.e., τ_1, τ_2, τ_3, and τ_4) for initial speeds of 20 – 65 mph is shown in Figure 5. The results are consistent at different speeds. The average of the time delay for each LCV unit is used for parameters τ_1, τ_2, τ_3, and τ_4 in the model.

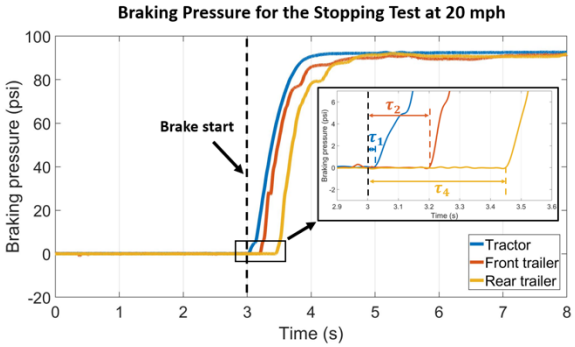

Figure 4. Brake pressure transient for straight-line braking tests at 20 mph

When the relay valve opens, the air is supplied to the brake chamber through the service line, as previously discussed in Figure 2. A first-order model is used to simulate the pressure transient in the brake chamber [8]:

$$p_{s\_tractor}(t) + T_{s\_tractor}\frac{dp_{s\_tractor}(t)}{dt} = p_{c\_tractor}(t) \quad (5)$$

$$p_{s\_trailerA}(t) + T_{s\_trailerA}\frac{dp_{s\_trailerA}(t)}{dt} = p_{c\_trailerA}(t) \quad (6)$$

$$p_{s\_dolly}(t) + T_{s\_dolly}\frac{dp_{s\_dolly}(t)}{dt} = p_{c\_dolly}(t) \quad (7)$$

$$p_{s\_trailerB}(t) + T_{s\_trailerB}\frac{dp_{s\_trailerB}(t)}{dt} = p_{c\_trailerB}(t) \quad (8)$$

where $p_{s\_i}(t)$ (*i= tractor, trailer A, dolly, and trailer B*) is the pressure in the brake chamber. The input for the above equations is the relay valve control pressure obtained from equations (1) - (4). In equations (5) - (8), $T_{s\_i}(t)$ is the time constant accounting for the pneumatic resistance of the service line, which is determined according to FMVSS 121 [27]. The FMVSS 121 spells out the requirements regarding brake actuation and release time for each vehicle unit in LCVs, as summarized in Table 2. The supply process is to charge the brake chamber to 85 psi within 0.2 second, and the release process is to discharge the chamber from 95 psi to 0 psi at the same rate.

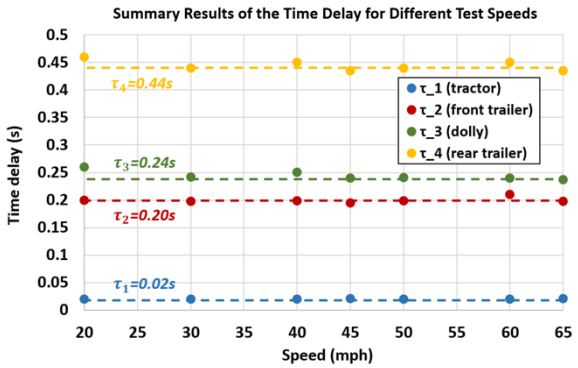

Figure 5. Maximum brake delay for tractor, front trailer, dolly, and rear trailer (τ_1, τ_2, τ_3, and τ_4) at various speeds

Table 2. FMVSS 121 requirements for brake actuation and release time delay, according to [27]

Vehicle unit	At the brake chamber	
	Apply (time to reach 60 psi)	Release (time to reach 5 psi)
Tractor	0.45 s	0.55 s
Dolly	0.55 s	1.10 s
Semi-trailer	0.50 s	1.00 s

To calculate the time constant, the first-order model that is assumed for the air transport is represented in the Laplace domain as:

$$\frac{P(s)}{U(s)} = \frac{1}{Ts+1} \quad (9)$$

Where P(s) is the pressure and U(s) is the input (in our case, the control line pressure). For instance, the pressure input according to FMVSS 121 requirement in the time domain is:

$$u(t) = \begin{cases} 425t & 0 \le t \le 0.2 \\ 85 & t > 0.2 \end{cases} \quad (10)$$

In the Laplace domain, the pressure input is:

$$U(s) = \int_0^{\frac{85}{425}} 425te^{-st}dt + \int_{\frac{85}{425}}^{\infty} 85e^{-st}dt = \frac{425}{s^2}\left(1 - e^{-s\frac{85}{425}}\right) \quad (11)$$

Substituting Equation (11) into Equation (9) gives:

$$P(s) = \frac{425(1-e^{-s\frac{85}{425}})}{s^2(Ts+1)} \quad (12)$$

Taking the inverse Laplace transform yields:

$$p(t) = 425t - 425T + 425(T - t - Te^{-\frac{(t-\frac{85}{425})}{T}} + \frac{85}{425}) + 425Te^{-\frac{t}{T}} \quad (13)$$

$p(t)$ and t need to be set at 60 and 0.45, respectively, as required by FMVSS 121 (Table 2). The time constant is then calculated to be 0.281. This method is applied to calculate the time constant, T, for brake actuation and release for each vehicle unit, as summarized in Table 3.

Table 3. The time constant, T, for brake application and release

	$T_{s\_tractor}$	$T_{s\_trailerA}$	T_{s_dolly}	$T_{s\_trailerB}$
Apply model	0.281	0.323	0.364	0.323
Release model	0.089	0.240	0.271	0.240

2.4 Brake Torque Modeling

The brake torque model is derived based on test data for S-cam drum brakes that are shown in Figure 6. The figure, derived from a study by Ashley et al. [5, 9, 10], shows the brake torque variations at 20, 50, and 60 mph for the steer axle, drive axle, and trailer axle of a tractor-trailer. The test results indicate that brake torque increases nearly linearly with brake chamber pressure. It also indicates that higher initial speeds result in lower brake torques. As discussed earlier, this is mainly due to the reduced coefficient of friction of the brake shoe material and drum brake radial expansion due to heating. Interestingly, the brake torques for various speeds are nearly the same for 20 psi chamber pressure.

During braking application, the brake pressure typically increases to 20 psi in a short time with minimal brake torque. Hence, the heat buildup at various speeds is negligible or nearly the same. It is therefore reasonable to model the brake torque vs. chamber pressure at various speeds such that they converge together at a chamber pressure of 20 psi, i.e., P_c=20 psi, as shown in Figure 7.

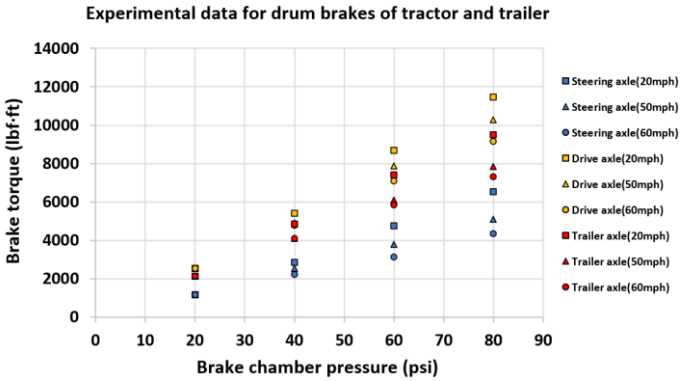

Figure 6. S-cam drum brake test data for steer, drive, and trailer axles

In Figure 7, the brake torque is modeled as a linear piecewise function of the brake chamber pressure [5, 9, 28], which is derived using four test data (red dots). The first dot is the pop-out pressure (P_0) that is typically set at 7 psi [5, 9, 28, 29], below which there is no brake torque since there is no or negligible contact between the brake shoes and drum. One can think of this as the minimum pressure to overcome the force of the return spring. For P_c>7 psi, brake torque increases linearly to M_{bc} (P_c=20 psi), which is the convergence point for various initial speeds. Test data in Figure 6 is modeled by linear lines with decreasing slops with increasing initial speed.

To determine the slope of the lines for speeds other than the two shown in Figure 7, one can interpolate between the two, as shown in Figure 8. The slope of the lines for 20 and 60 mph in Figure 7 can be determined as:

$$a_{20} = \frac{M_{b20} - M_{bc}}{60} \tag{14}$$

$$a_{60} = \frac{M_{b60} - M_{bc}}{60} \tag{15}$$

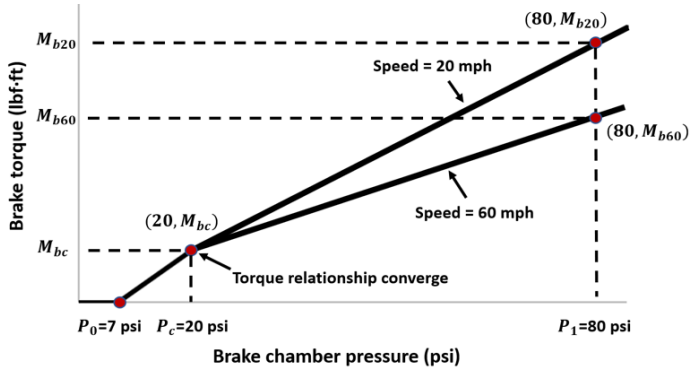

Figure 7. Piecewise linear representation of brake torque versus chamber pressure at 20 and 60 mph initial speeds

Using the above, the linear relationship for the slope coefficient (a) versus the initial speed can be determined as:

$$a = \left(\frac{a_{60} - a_{20}}{40}\right)(V_{x0} - 60) + a_{60} \tag{16}$$

where V_{x0} is the initial speed (i.e., the speed when the brake is applied).

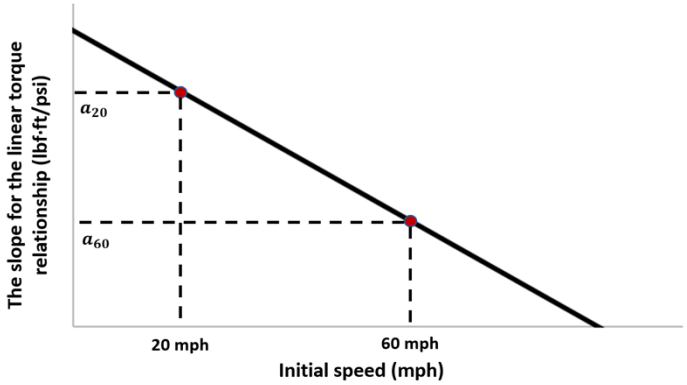

Figure 8. Linear interpolation of the slope of brake torque vs. brake pressure in Figure 7

Then, the brake torque can be written as a function of chamber pressure and initial speed:

$$M_b = a(P_{s_i} - 20) + M_{bc} = \left[\left(\frac{a_{60} - a_{20}}{40}\right)(V_{x0} - 60) + a_{60}\right](P_{s_i} - 20) + M_{bc} \tag{17}$$

The piecewise function to calculate the brake torque is finally determined as:

$$M_b = \begin{cases} 0 & (0 \le P_{s_i} \le P_0) \\ \frac{(P_{s_i} - 7)}{13} M_{bc} & (P_0 < P_{s_i} \le P_c) \\ \left[\left(\frac{M_{b60} - M_{b20}}{2400}\right)(V_{x0} - 60) + \frac{M_{b60} - M_{bc}}{60}\right](P_{s_i} - 20) + M_{bc} & (P_c < P_{s_i}) \end{cases} \tag{18}$$

where M_b is the brake torque and P_{s_i} is the pressure in the brake chamber. The parameters M_{b20}, M_{b60}, and M_{bc}, provided in Table 4, are determined from the test data in Figure 6.

Table 4. Parameters used for the brake torque modeling of the LCV

Parameter	Steering axle	Drive axle	Trailer/ dolly axle
M_{bc} (lbf·ft)	1174.9	2482.8	2140.4
M_{b20} (lbf·ft)	6531.6	11540.2	9473.7
M_{b60} (lbf·ft)	4368.2	9241.4	7280.7

Figures 9a-9c compare the model's prediction with test results for speeds ranging from 20 to 60 mph for the steering axle, drive axle, and trailer/dolly axle. The lines represent the results from equation (18), and the dots represent the test data for some of the speeds that were tested

in [5, 9, 10]. A good agreement between the model and test data is observed, with a difference of less than 5.4%, 6.4%, and 6.3% for the steering axle, driver axle, and trailer/dolly axle, respectively. The results in Figure 9 also indicate that the largest and smallest brake torques are generated at the drive axle and steering axle, respectively.

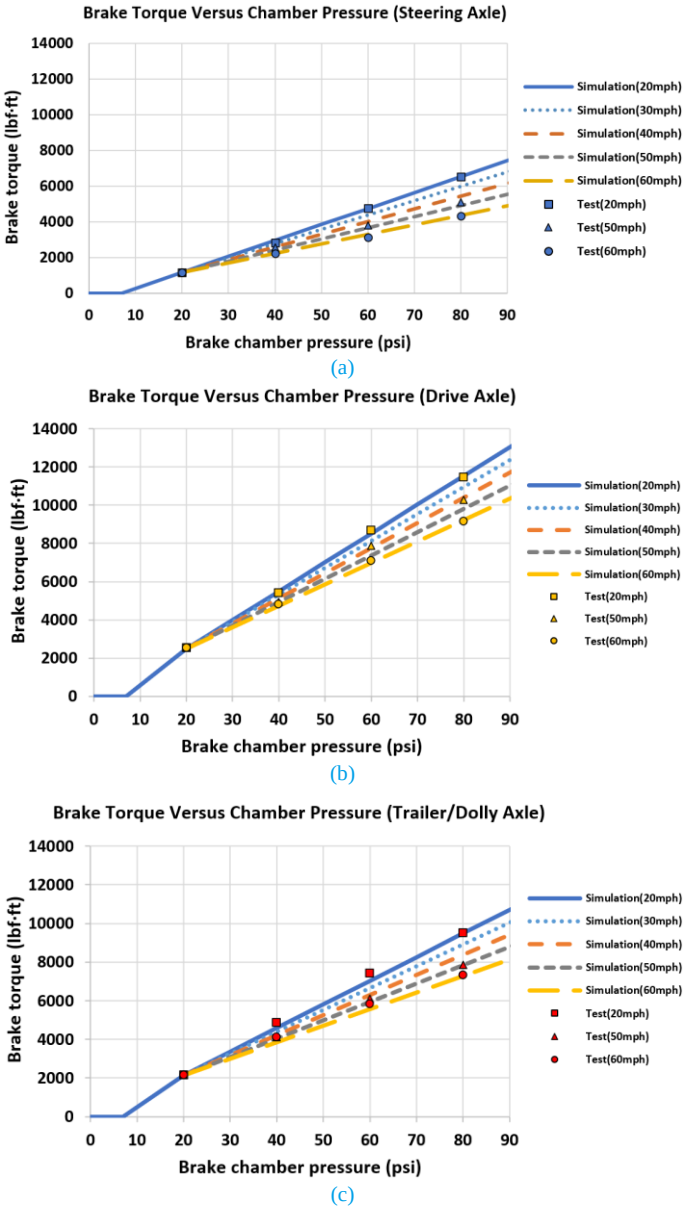

Figure 9. Comparison of simulation results and test data for brake torque versus chamber pressure at various initial speeds; (a) steer axle, (b) drive axle, and (c) trailer/dolly axle (c)

2.5 Anti-lock Brake System (ABS) Modeling

The effect of the anti-lock brake system (ABS), which has been mandated for commercial trucks [10, 30], is also included in the study. Modeling the ABS requires a knowledge of its working principle (i.e., how to prevent the wheel lockup and maximize the braking effort). Using the wheel configuration in Figure 10, one can model the wheel motion as [19, 31]:

$$I_w\dot{\omega} = F_xR_t - M_b \tag{19}$$

where I_w is the wheel inertia, $\dot{\omega}$ is the angular acceleration, F_x is the braking force, R_t is the tire radius, and M_b is the brake torque. For large M_b (i.e., hard braking) and/or small F_x (slippery road surface), the wheel decelerates quickly and eventually locks up, causing sliding. This can increase braking distance and time, and possibly lead to understeering or jackknifing [32]. The ABS intervenes before wheel lockup by releasing the brake chamber pressure to reduce brake torque, M_b.

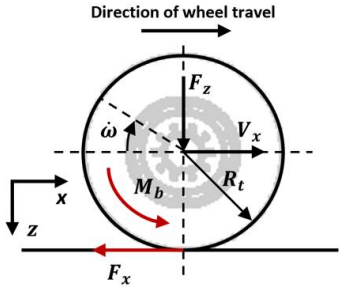

Figure 10. Wheel rotational dynamics during braking

By modulating the brake chamber pressure, the ABS can maintain the wheel slip ratio,

$$\kappa = \frac{V_x - \omega R_t}{V_x} \tag{20}$$

near the range that provides maximum braking force [33] and [11]. The term κ is the slip ratio, V_x is the vehicle driving speed, ω is the wheel angular velocity, and R_t is the wheel radius. At wheel lockup (i.e., ω= 0), the slip ratio becomes 1, i.e., $\kappa = 1$, The braking force can be calculated as:

$$F_x = \mu_x F_z \tag{21}$$

where F_x is the braking force, F_z is the wheel load, and μ_x is the braking coefficient (also referred to as "normalized braking traction"). Figure 11 shows the change in braking coefficient with slip ratio at the 4,000 lb. wheel load. The dry road braking coefficient is calculated from the test data in [34]. The wet road braking coefficient is calculated from the similarity method proposed by Pacejka, using the dry road data [2, 35].

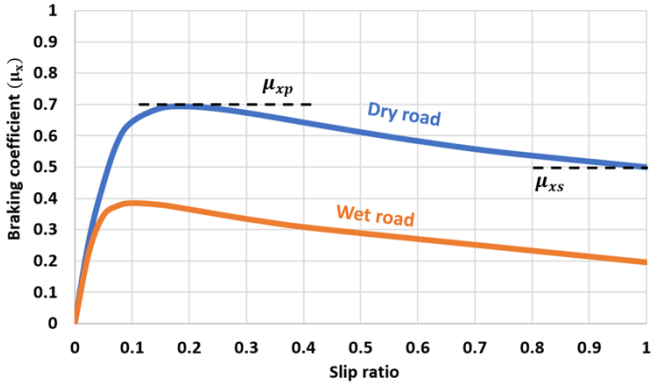

Figure 11. Braking coefficient versus slip ratio (wheel load=4000 lb)

As shown in Figure 11, the sliding coefficient, μ_{xs}, is lower than the peak braking coefficient, μ_{xp}, for both the dry and wet roads. Figure 11 also indicates that the peak braking coefficient, μ_{xp}, occurs in the range of 0.1 (for wet roads) to 0.2 (for dry roads). This agrees with other studies that have investigated ABS control [36, 37]. Therefore, for this study, the ABS is modeled as a module that is activated to release brake chamber pressure when detecting a slip ratio that is larger than 0.2. The ABS control is terminated when the slip ratio drops below 0.1.

3. Integration into LCV Dynamics Model

The pneumatic brake system model is developed in Simulink®, with the blocks shown in Figure B1 in Appendix B. The Simulink® model is integrated into a TruckSim® model for a 33-ft A-double, as shown in Figure 12, using a co-simulation approach.

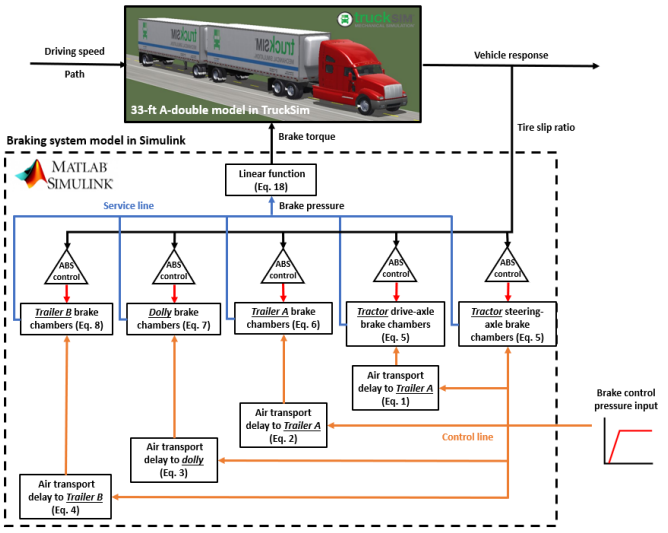

Figure 12. TruckSim®-Simulink® co-simulation architecture

For the co-simulation, the Simulink® receives the slip ratio from the TruckSim® while feeding the TruckSim® with the brake torque. The input necessary for the co-simulation includes the driving speed, a predetermined path in TruckSim®, and the brake control pressure in Simulink®. The 33-ft A-double is assumed to be at the Federal limit of 80,000 lb. gross vehicle weight (GVWT), with the two trailers equally loaded [38]. Table A1 summarizes the parameters used for the model. The non-linear braking force characteristics of the tire used in the simulation are provided in Figure 13, which is obtained from the test data by the University of Michigan Transportation Research Institute (UMTRI) for a truck tire with $\mu_{xp} = 0.9$ [34]. The details of the TruckSim® model can be found in the authors' past publications, for instance [2, 22, 39].

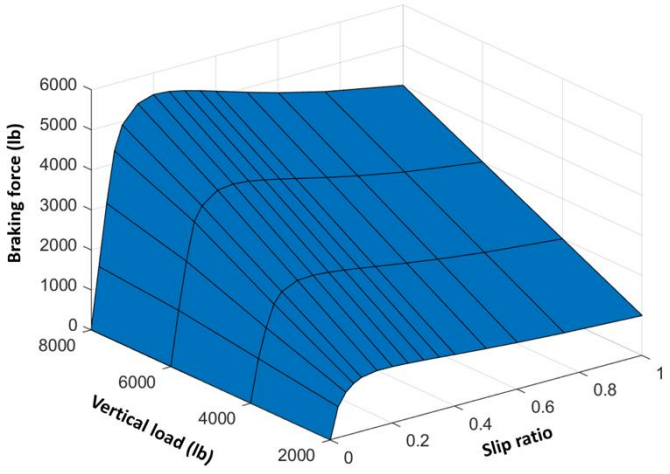

Figure 13. Tire force characteristics used for dynamic simulations

4. Comparison with Test Data

The truck model is validated by comparing the results with track-test data for straight-line braking. The straight-line braking emulates hard stopping, without steering, such as what may be needed for avoiding a stopped vehicle ahead.

4.1 Straight-line Stopping Test

The straight-line stopping tests were performed by the Center for Vehicle Systems and Safety at Virginia Tech. The tests were conducted with the 2004 Volvo tractor and two 33-ft trailers shown in Figure 14. The tractor, trailers, and converter dolly were all equipped with drum brakes. A global positioning system (GPS) was used to log the vehicle's speed beyond the tractor's speedometer. The longitudinal deceleration of the tractor and trailers were also recorded by accelerometers mounted near the CG position of the vehicles. We also measured the pressures within the brake chambers for the tractor and two trailers. A braking robot was used for the tests to ensure repeatable and accurate brake pedal applications across the multitude of tests that were performed. The robotic braking was initiated automatically through an optical trigger placed at a demarcation line. The test speeds were from 20 to 65 mph, with each speed repeated three times. The drum temperature was measured after the three tests for each speed and two cool-down laps of approximately 2 miles were performed in between the tests to maintain the brake temperature for each speed within a controlled range.

Figure 14. 33-ft A-double used for straight-line stopping tests

4.2 Straight-line Stopping Comparison at 40 mph

Full braking, for which the brake control pressure increases to 85 psi in 0.2 s as per the FMVSS 121 [27], is applied, as shown in Figure 15. The brake pressures, vehicle velocity, and decelerations from the model are compared with the test results for an initial speed of 40 mph, as shown in Figures 16 and 17. It should be noted that a pavement coefficient of friction of 0.8 is used for the model, corresponding to the dry asphalt at the test track [40].

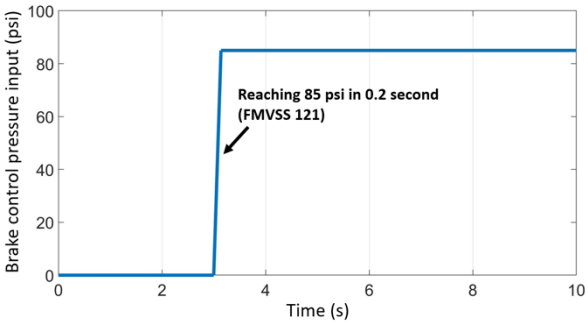

Figure 15. Brake control pressure input for simulation model validation

A good agreement is observed between the simulation results and test data, as shown in Figures 16 and 17 for the brake pressure, speed, and longitudinal deceleration of the tractor and trailers. The time delay (defined as the initiation of braking at the pedal to final pressure at the

chamber) agrees extremely well for the tractor and trailers at various axles, as shown in Figure 16. This is critical to accurately capturing the sequential delay in braking that exists in LCVs. Additionally, the brake pressure fluctuations associated with the ABS are accurately represented in the model. It shows the brake pressure fluctuating between 85 psi and 40 psi in multiple cycles.

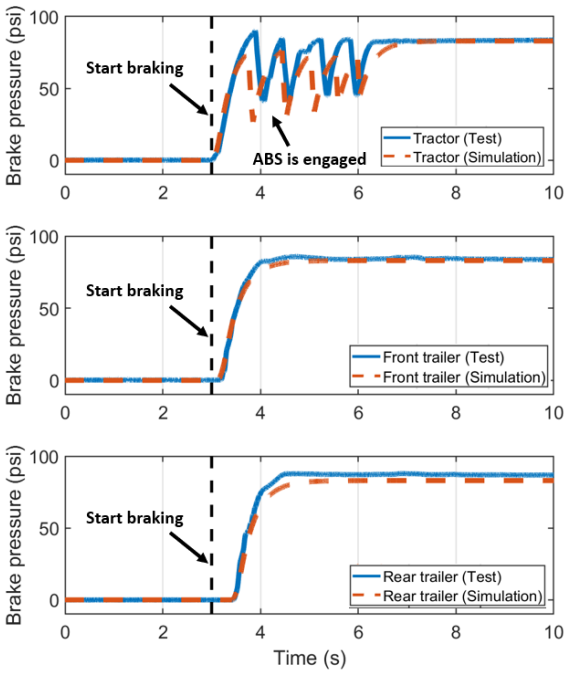

Figure 16. Simulation and test results comparison of brake pressure for straight-line braking at 40 mph for tractor, front trailer, and rear trailer

The figure shows the agreement between the simulation results and test data for speed reduction and longitudinal deceleration of the tractor and trailers. The results for this specific speed (40 mph) prove the accuracy of the model in predicting the truck's deceleration during braking. Notably, the tractor, front trailer, and rear trailer exhibit nearly the same change in the longitudinal deceleration, as would be expected. The steady-state value of the deceleration stays around 0.6 g, which is close to the experimental measurements from Garrott et al. [41] and Bedsworth et al. [42] on a tractor-semitrailer with 80,000 lb. gross weight.

4.3 Braking Distance and Braking Time Modeling

To further validate the model, the braking distance and braking time at 20 to 65 mph are compared with the test-track results. The braking distance is defined as the distance that a vehicle will travel to come to a full stop after the brake is fully applied [43]. The braking time is the period that it takes for the LCV to stop. The braking distance is also referred to as the minimum distance to avoid an obstacle by braking (commonly known as "the last point to brake" [44]). If the driver brakes to prevent colliding with an obstacle at a distance less than the braking distance, the collision is most likely unavoidable. As shown in Figure 18, the braking distance is not the same as the stopping distance. Braking distance refers to the distance available for braking from where the driver applies the brakes to where the obstacle is located. The stopping distance is the braking distance plus the distance traveled during the driver perception/reaction (PR) time.

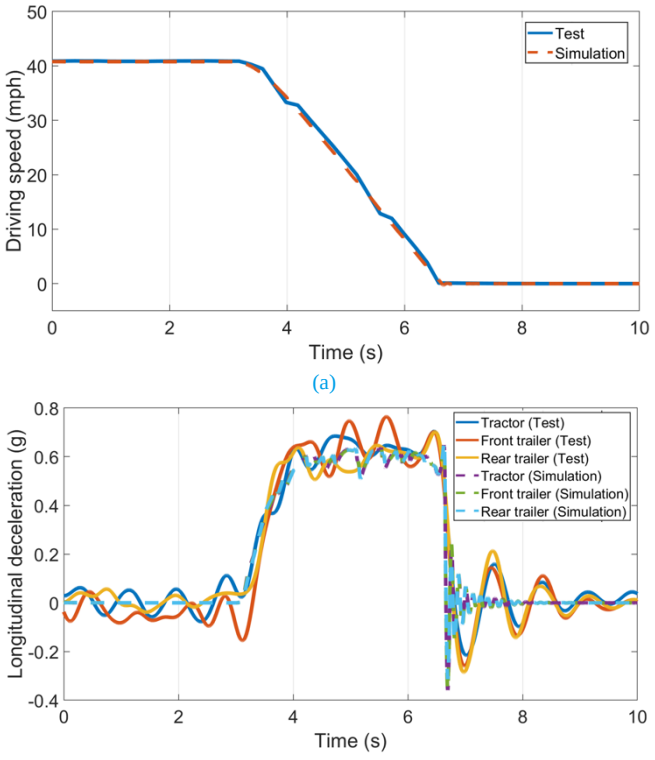

Figure 17. Simulation and test results comparison for straight-line braking at 40 mph; (a) vehicle speed, (b) tractor, front trailer, and rear trailer decelerations

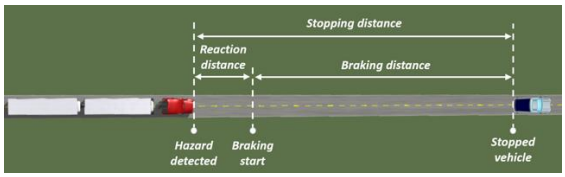

Figure 18. Braking distance and stopping distance schematic

Assuming a constant braking deceleration, one can calculate the braking distance, d_s , as, [11, 45]:

$$d_s = \frac{F_x}{m} = \frac{{V_{x0}}^2 - {V_{xf}}^2}{2a_x} \quad (22)$$

where a_x is the longitudinal deceleration, F_x is the total braking force, m is the vehicle mass, V_{x0} and V_{xf} are the initial and final speeds, respectively, and d_s is the braking distance. For full stop, $V_{xf} = 0$, and Eq. (22) simplifies to:

$$d_s = \frac{{V_{x0}}^2}{2a_x} \quad (23)$$

The braking time (t_s) to a full stop is:

$$t_s = \frac{V_{x0}}{a_x} \quad (24)$$

The equations above indicate that the braking time increases in direct proportion to the initial speed, whereas the braking distance is directly proportional to the second power of the initial speed. Figure 19 shows the straight-line braking distance versus speed, according to track tests and simulations. The actual test speeds might differ from the target speeds, but the difference is less than 1 mph. The simulation results closely match the field tests, with a difference of less than 7.1%. As speed increases from 20 to 65 mph, the braking distance increases by approximately 800%, which is in line with Equation (23). Interestingly,

for higher speeds (>55 mph), the braking distance is less consistent for repeated tests. This is mainly attributed to the increase in brake temperature and any fading that it may cause, as was discussed earlier.

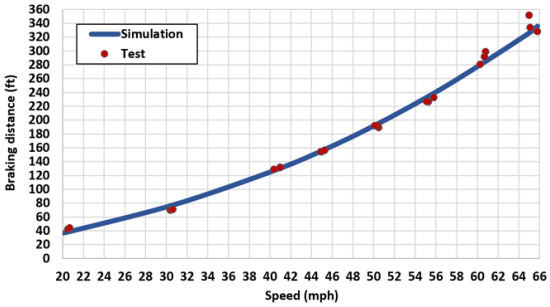

Figure 19. Comparison of simulation results with field tests for straight-line braking distance at 20 to 65 mph

The braking time results are shown in Figure 20. Good agreement is observed between the tests and simulation at various speeds. The simulation results are within 2.4 % of the test data, with a nearly linear trend as suggested by Eq. (24). The braking time increases by approximately 180% from 20 to 65 mph, which is far less than the increase in braking distance. Overall, the excellent agreement between the simulation results and test data at various speeds suggests that the model can be used confidently to predict the stopping distance and time for LCVs under various driving conditions.

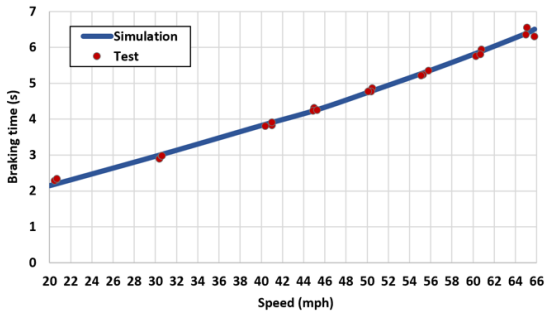

Figure 20. Comparison of brake-time simulation and test results for straight-line braking from 20 to 65 mph

5. Effect of Road Condition on Braking

As a case study, we evaluate the effect of the road coefficient of friction, μ_p , on braking, using the model. The μ_p is assumed to vary from 0.3 – 0.9 (changed in 0.1-increments) to represent a range of conditions from snowy to wet to dry roads [46]. For each, the stopping distance and time are evaluated at 20 – 65 mph initial speeds, as shown in Figure 21. The braking distance increases non-linearly with speed for nearly all road friction. On slippery roads, (lower μ_p), the increase in stopping distance appears to be nearly linear with speed. This is mainly attributed to lower braking force and deceleration on more slippery roads. The results indicate that braking time increases almost linearly with speed for all road conditions. The slippery roads result in a longer time to stop mainly due to lower braking force at the pavement and possible activation of the ABS. At a given speed, the time to stop increases nonlinearly as μ_p decreases. For instance, at 55 mph when μ_p decreases from 0.9 to 0.8 and again from 0.8 to 0.7, the time to stop increases by a fraction of one second only. Decreasing μ_p by the same 0.1 from 0.4 to 0.3, however, increases the time to stop by nearly four seconds. This indicates that the initial speed plays a far more critical role in stopping time and distance on roads with a lower coefficient of friction.

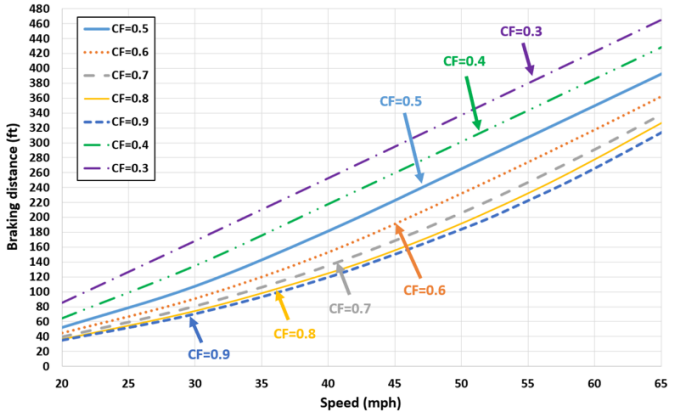

(a)

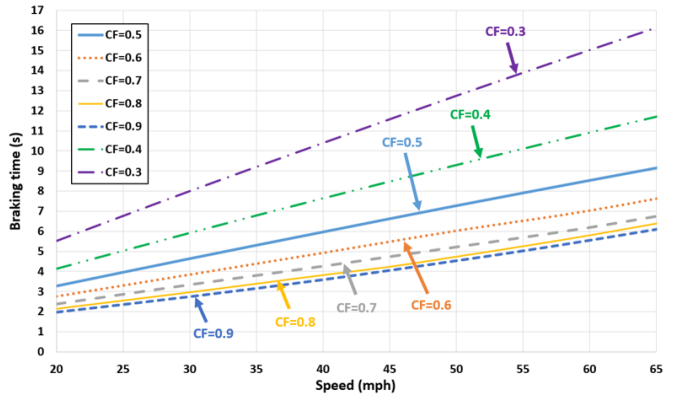

(b)

Figure 21. Effect of road condition on braking for various pavement coefficient of friction, μ_p; (a) braking distance, (b) braking time

6. Concluding Remarks

A detailed description of the development of a pneumatic brake model that accounts for accurate braking dynamics of 33-ft A-doubles that are classified as long combination vehicles (LCVs) was provided. The developed brake model was integrated into the truck's multi-body dynamic model in TruckSim® through a co-simulation technique. The simulation prediction of braking distance and time at different speeds (20 to 65 mph) matched well with track-testing results, to within 7.1% (braking time) and 2.4% (braking distance). The excellent agreement between the simulation and straight-line testing proves the accuracy and effectiveness of the detailed brake dynamic model that is developed for the study. The model includes the critical factors affecting braking time and distance such as brake delay and fading with far higher accuracy than documented in the past studies. A case study was carried out to demonstrate the utility of the model. The effect of pavement coefficient of friction, μ_p, on braking was evaluated in the case study. As expected, stopping distance increases nonlinearly with the initial speed, whereas stopping time increases nonlinearly. For lower μ_p, the increase in stopping distance, however, is nearly linear with the initial speed. This was attributed to the lower achievable maximum braking force with smaller μ_p. At a given initial speed, the results indicated that as μ_p decreases, stopping time increases nonlinearly. A similar effect is observed for stopping distance, but with a far lesser degree of nonlinearity. The agreement between the simulation and test results further proves that the model can be used confidently for parametric studies beyond those considered here.

References

[1] A. Grislis, "Longer combination vehicles and road safety," *Transport*, vol. 25, no. 3, pp. 336-343, 2010.

[2] Y. Chen, Z. Zhang, and M. Ahmadian, "Comparative Analysis of Emergency Evasive Steering for Long Combination Vehicles," *SAE Int. J. Commer. Veh*, vol. 13, no. 3, 2020.

[3] S. C. Subramanian, S. Darbha, and K. R. Rajagopal, "Modeling the pneumatic subsystem of an S-cam air brake system," *J. Dyn. Sys., Meas., Control*, vol. 126, no. 1, pp. 36-46, 2004.

[4] S. Williams and R. R. Knipling, "Automatic Slack Adjusters for Heavy Vehicle Air Brake Systems. Final Report," 1991.

[5] A. L. Dunn, "Jackknife stability of articulated tractor semitrailer vehicles with high-output brakes and jackknife detection on low coefficient surfaces," The Ohio State University, 2003.

[6] R. He and Z. Jing, "Study on braking stability of commercial vehicles: An optimized air brake system," *Advances in Mechanical Engineering*, vol. 11, no. 5, p. 1687814019848593, 2019.

[7] T. Qin, G.-Y. Li, M. Tu, and T. Wu, "Bus pneumatic braking circuit delay analysis and control," *Transactions of Beijing Institute of Technology*, vol. 32, no. 5, pp. 470-474, 2012.

[8] Z. Wang, X. Zhou, C. Yang, Z. Chen, and X. Wu, "An experimental study on hysteresis characteristics of a pneumatic braking system for a multi-axle heavy vehicle in emergency braking situations," *Applied Sciences*, vol. 7, no. 8, p. 799, 2017.

[9] A. L. Dunn, G. J. Heydinger, G. Rizzoni, and D. A. Guenther, "Empirical models for commercial vehicle brake torque from experimental data," *SAE transactions*, pp. 1455-1466, 2003.

[10] A. L. Dunn, G. Heydinger, G. Rizzoni, and D. Guenther, "In-depth analysis of the influence of high torque brakes on the jackknife stability of heavy trucks," *SAE transactions*, pp. 255-272, 2003.

[11] T. D. Gillespie, *Fundamentals of vehicle dynamics*. Society of automotive engineers Warrendale, PA, 1992.

[12] S. Mithun, S. Mariappa, and S. Gayakwad, "Modeling and simulation of pneumatic brake system used in heavy commercial vehicle," *IOSR Journal of Mechanical and Civil Engineering*, vol. 11, no. 1, pp. 1-9, 2014.

[13] S. C. Subramanian, S. Darbha, and K. Rajagopal, "A diagnostic system for air brakes in commercial vehicles," *IEEE transactions on intelligent transportation systems*, vol. 7, no. 3, pp. 360-376, 2006.

[14] T. Acarman, U. Ozguner, C. Hatipoglu, and A.-M. Igusky, "Pneumatic brake system modeling for systems analysis," SAE Technical Paper, 0148-7191, 2000.

[15] F. Bu and H.-S. Tan, "Pneumatic brake control for precision stopping of heavy-duty vehicles," *IEEE Transactions on Control Systems Technology*, vol. 15, no. 1, pp. 53-64, 2006.

[16] J. Wu, H. Zhang, Y. Zhang, and L. Chen, "Robust design of a pneumatic brake system in commercial vehicles," *SAE International Journal of Commercial Vehicles*, vol. 2, no. 2009-01-0408, pp. 17-28, 2009.

[17] S. Palanivelu, J. Patil, and A. K. Jindal, "Modeling and optimization of pneumatic brake system for commercial vehicles by model based design approach," SAE Technical Paper, 0148-7191, 2017.

[18] C. Chen, G. Wagner, M. Pace, and T. Rogness, "Prediction of heavy truck stopping distance and vehicle behavior using real-time HIL and SIL simulation," SAE Technical Paper, 0148-7191, 2008.

[19] M.-W. Suh, Y.-K. Park, S.-J. Kwon, S.-H. Yang, and B.-C. Park, "A simulation program for the braking characteristics of tractor-semitrailer vehicle," *SAE transactions*, pp. 540-550, 2000.

[20] Y. Chen, A. W. Peterson, C. Zhang, and M. Ahmadian, "A simulation-based comparative study on lateral characteristics of trucks with double and triple trailers," *International Journal of Vehicle Safety*, vol. 11, no. 2, pp. 136-157, 2019.

[21] R. R. Knipling, "Twin 33 Foot Truck Trailers: Making U.S. Freight Transport Safer And More Efficient," 2016. [Online]. Available: https://americansformoderntransportation.org/wp-content/uploads/Ron-Knipling-Twin-33-Study-vF.pdf.

[22] Y. Chen, Zheng, X., Peterson, A., Ahmadian, M., "Simulation Evaluation on the Rollover Propensity of Multi-trailer Trucks at Roundabouts," *SAE technical paper*, 2020, Art no. 2020-01-5005, DOI: 10.4271/2020-01-5005.

[23] S. C. Subramanian, S. Darbha, and K. R. Rajagopal, "Developing a diagnostic system for air brakes used in commercial vehicles," 2006.

[24] S. G. Insurance. "Air Brake Manual." https://www.sgi.sk.ca/documents/625510/626984/airbrake_manual.pdf/1601c666-44bf-4078-a1ae-97d436440885 (accessed 2021).

[25] Y. Chen, A. W. Peterson, and M. Ahmadian, "Achieving anti-roll bar effect through air management in commercial vehicle pneumatic suspensions," *Vehicle System Dynamics*, vol. 57, no. 12, pp. 1775-1794, 2019.

[26] Y. Chen, M. Ahmadian, and A. Peterson, "Pneumatically balanced heavy truck air suspensions for improved roll stability," SAE Technical Paper, 0148-7191, 2015.

[27] N. H. T. S. Administration, "Federal Motor Vehicle Safety Standards; Air Brake Systems. 49 CFR Part 571, Docket No," NHTSA–2009-0083, 2009.

[28] R. L. Hoover and S. B. Zagorski, "Comparison of Heavy Truck Foundation Brake Performance measured with an Inertia Brake Dynamometer and Analyses of Brake Output Responses to Dynamic Pressure Inputs," SAE Technical Paper, 0148-7191, 2005.

[29] B. C. Zaugg, G. J. Heydinger, D. A. Guenther, A. L. Dunn, S. B. Zagorski, and P. A. Grygier, "The development of a heavy truck ABS model," *SAE transactions*, pp. 12-27, 2005.

[30] S. B. Zagorski, "Compatibility of ABS disc/drum brakes on class VIII vehicles with multiple trailers and their effects on jackknife stability," The Ohio State University, 2004.

[31] M. Suh, Y. Park, and S. Kwon, "Braking performance simulation for a tractor-semitrailer vehicle with an air brake system," *Proceedings of the Institution of Mechanical Engineers, Part D: Journal of Automobile Engineering*, vol. 216, no. 1, pp. 43-54, 2002.

[32] B. Li and S. Rakheja, "Jackknifing Prevention of Tractor-Semitrailer Combination Using Active Braking Control," SAE Technical Paper, 0148-7191, 2015.

[33] T. D. Day and S. G. Roberts, "A simulation model for vehicle braking systems fitted with ABS," *SAE Transactions*, pp. 821-839, 2002.
[34] P. S. Fancher, "Generic data for representing truck tire characteristics in simulations of braking and braking-in-a-turn maneuvers. Final report," 1995.
[35] H. B. Pacejka and R. S. Sharp, "Shear force development by pneumatic tyres in steady state conditions: a review of modelling aspects," *Vehicle system dynamics*, vol. 20, no. 3-4, pp. 121-175, 1991.
[36] F. Chikhi, A. El Hadri, and J.-C. Cadiou, "ABS control design based on wheel-slip peak localization," in *Proceedings of the Fifth International Workshop on Robot Motion and Control, 2005. RoMoCo'05.*, 2005: IEEE, pp. 73-77.
[37] N. Patra and K. Datta, "Sliding mode controller for wheel-slip control of anti-lock braking system," in *2012 IEEE International Conference on Advanced Communication Control and Computing Technologies (ICACCCT)*, 2012: IEEE, pp. 385-391.
[38] F. H. A. U. S. D. o. Transportation, "Compilation of Existing State Truck Size and Weight Limit Laws," 2015. [Online]. Available: https://ops.fhwa.dot.gov/freight/policy/rpt_congress/truck_sw_laws/truck_sw_laws.pdf
[39] Y. Chen, Y. Hou, A. Peterson, and M. Ahmadian, "Failure mode and effects analysis of dual leveling valve airspring suspensions on truck dynamics," *Vehicle system dynamics*, vol. 57, no. 4, pp. 617-635, 2019.
[40] NHTSA, "Tractor Semi-Trailer Stability Objective Performance Test Research – Roll Stability," 2011. Accessed: Jan/2020. [Online]. Available: https://www.nhtsa.gov/sites/nhtsa.dot.gov/files/811467.pdf
[41] W. R. Garrott, M. Heitz, and B. Bean, "Experimental measurement of the stopping performance of a tractor-semitrailer from multiple speeds," *Accident reconstruction journal*, vol. 22, no. 3, pp. 45-57, 2012.
[42] K. Bedsworth, R. Butler, G. Rogers, K. Breen, and W. Fischer, "Commercial vehicle skid distance testing and analysis," SAE Technical Paper, 0148-7191, 2013.
[43] P. Greibe, "Braking distance, friction and behaviour," *Trafitec, Scion-DTU*, 2007.
[44] A. Eckert, B. Hartmann, M. Sevenich, and P. Rieth, "Emergency steer & brake assist: a systematic approach for system integration of two complementary driver assistance systems," in *22nd International Technical Conference on the Enhanced Safety of Vehicles (ESV)*, 2011, pp. 13-16.
[45] P. Delaigue and A. Eskandarian, "A comprehensive vehicle braking model for predictions of stopping distances," *Proceedings of the Institution of Mechanical Engineers, Part D: Journal of Automobile Engineering*, vol. 218, no. 12, pp. 1409-1417, 2004.
[46] A. A. Kordani, O. Rahmani, A. S. A. Nasiri, and S. M. Boroomandrad, "Effect of adverse weather conditions on vehicle braking distance of highways," *Civil Engineering Journal*, vol. 4, no. 1, pp. 46-57, 2018.

Abbreviations

LCV	Long combination vehicle	**FMVSS**	Federal Motor Vehicle Safety Standards
US	United States	**ABS**	Anti-lock braking system
TMC	Technology and Maintenance Council	**CG**	Center of gravity
GPS	Global positioning system	**OH**	Ohio
CF	Coefficient of friction		

Appendix A

Table A1. Parameters used for the braking dynamic simulation of the 33-ft A-double

Tractor		**Trailer**		**Dolly**	
Parameter	**Value**	**Parameter**	**Value**	**Parameter**	**Value**
Sprung weight	15882 lb	Trailer tare weight	10110 lb	Sprung weight	1527 lb
Roll moment of inertia	168435 lb·ft2	Loaded trailer weight	25110 lb	Roll moment of inertia	28488 lb·ft2
Pitch moment of inertia	515530 lb·ft2	Roll moment of inertia	403219 lb· ft2	Pitch moment of inertia	35612 lb·ft2
Yaw moment of inertia	511932 lb·ft2	Pitch moment of inertia	2990579 lb· ft2	Yaw moment of inertia	41663 lb·ft2
Wheelbase	255 in	Yaw moment of inertia	2913493 lb· ft2	Axle track	77 in
Steering axle track	77 in	Wheelbase	331 in	CG height to the ground	35.4 in
Drive axle track	77 in	Axle track	77 in	Dual tire lateral spacing	12 in
Dual tire lateral spacing	12 in	CG Long. to kingpin	171.1 in	CG Long. to kingpin	31.5 in
CG long. to kingpin	127.3 in	CG height to the ground	79.5 in	Wheelbase	72 in
CG height to the ground	39.8 in	Dual tire lateral spacing	12 in		

Appendix B

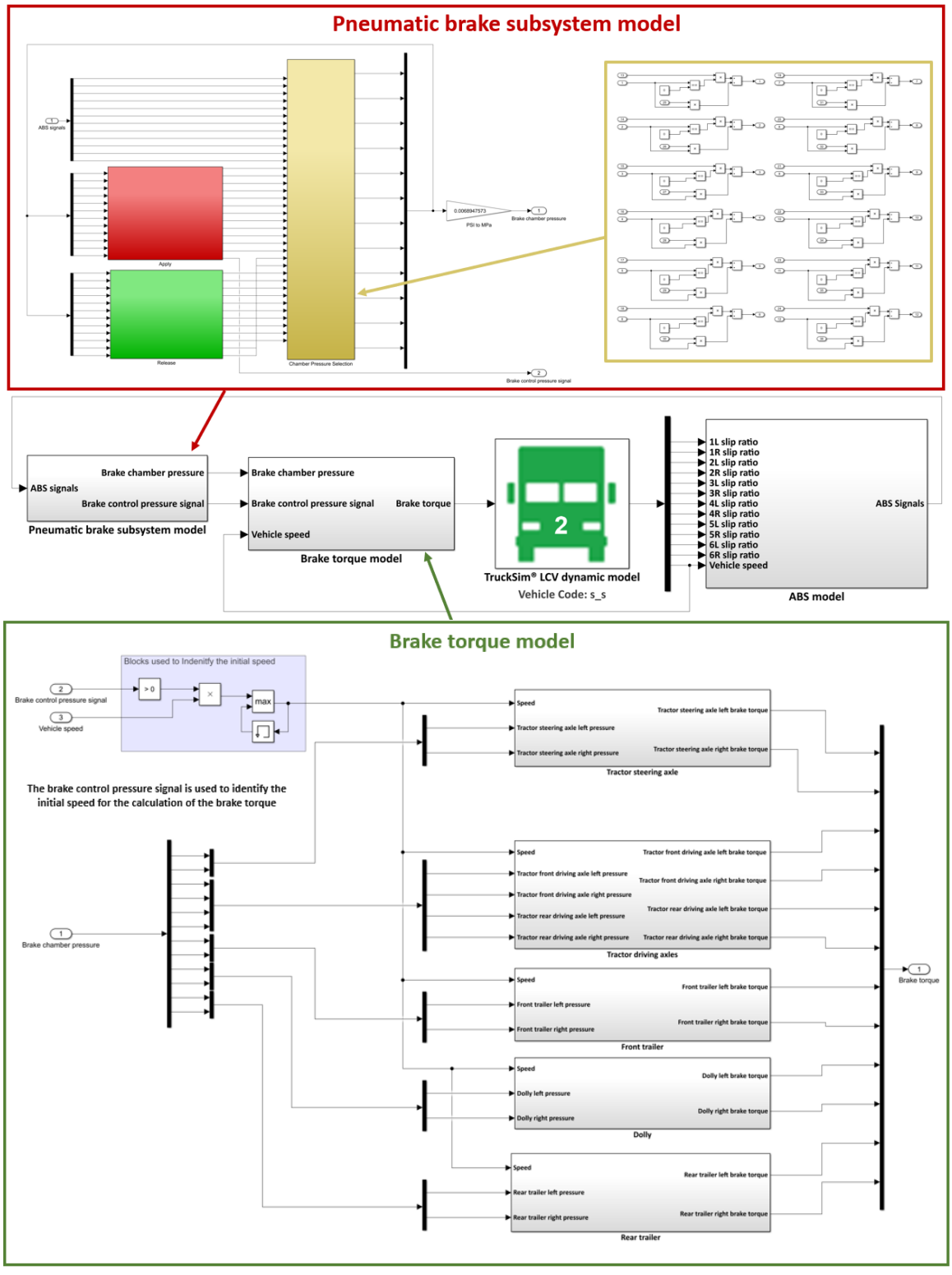

Figure B1. Co-simulation model established in Simulink® for predicting the braking dynamics for the 33-ft A-double